

EXPERIMENTAL DATA FROM A RADIO-CONTROLLED HELICOPTER FOR FLOW FIELD VALIDATION OF CFD SIMULATION

PJ Skinner and K Naidoo
Defence Aeronautics Programme, Defencetek, CSIR
pskinner@csir.co.za, knaidoo@csir.co.za

Abstract

Wind tunnel measurements of the flow field in the rotor downwash of a tethered commercial radio controlled helicopter are presented. A rapid response 5-hole probe was used for the measurements in hover and trimmed forward flight conditions. First order comparisons are presented between the wind tunnel measurements and first order accurate viscous Navier-Stokes solutions for hover and forward flight. The suitability of such scale models as validation vehicles for numerical simulations is discussed in the light of the experience gained. The results indicate that such models may be useful as validation vehicles if issues relating to the low level of signals from such small models are addressed.

Nomenclature

A	= area, m ²
c _{ref}	= reference chord, m
CFD	= Computational Fluid Dynamics
D	= rotor diameter, m
f _{l_w}	= wind axis lift force, N
m _{rc}	= moment reference centre
N	= number of blades
p _s	= static pressure, Pa
R	= rotor radius, m
RC	= Radio Control
t _{pp}	= tip path plane
V _{mag}	= velocity magnitude, m/s
w	= vertical velocity component (downwash), positive upwards
WT	= wind tunnel
α	= Angle of Attack, °
β	= Angle of Sideslip, °
ρ	= air density, kg/m ³
ω	= rotation speed, rad/s
μ	= advance ratio, V/ω R

$$C'_T = \text{thrust coefficient, } \frac{f_{l_w}}{\rho A (\omega R)^2}$$
$$\sigma = \text{solidity, } N \text{ cref} / \pi R$$

Introduction

The capabilities of numerical simulations continue to increase. Commercially available Computational Fluid Dynamics (CFD) codes are capable of simulating the entire helicopter domain including fuselage, main rotor with cyclic, and tail rotor. The ability of CFD to offer the whole flow field in the solution makes this capability all the more attractive. There are, however, known limits of the suitability of Navier-Stokes solvers in addressing complex flow fields with high vorticity content. It is therefore desirable to establish the limitations of lower order Navier-Stokes solvers as applied to helicopter simulations in the current context.

Detailed full scale flow field surveys are not usually a realistic option and high end commercial radio controlled (RC) helicopters offer the potential of relatively low cost validation vehicles for equivalent CFD models. Recent work on rotorcraft wakes at CSIR (Ref 1) saw the use of such RC helicopters and it was a logical extension to explore their potential as validation vehicles through the use of flow field surveys with a multi-hole probe.

A limited series of flow field surveys was conducted using a tethered RC helicopter in simulated hover and forward flight conditions. These were assessed in terms of their consistency and quality in the wind tunnel environment. Comparisons are presented between the wind tunnel measurements and first-order accurate numerical predictions from STAR-CD.

The objective is to assess the suitability of commercial RC helicopters as validation vehicles for numerical simulations and to develop insight into the limitations of STAR-CD for helicopter flow field applications.

Test Apparatus

The experiments were done in the Seven Metre Wind-tunnel (7.5mx6.5m) at the CSIR. This is a closed test section, open return facility. The model used was a fully articulated 46-scale RC model of the Agusta A109 helicopter.

The four bladed main rotor rotated in the clockwise sense when viewed from above. The blades were made from glass fibre and had a 21% cut-out and up to 94% radius had constant chord (48mm); constant thickness (~16%); and zero twist. The blade tips comprised 2-stage compound linear taper providing a rotor diameter of 1318mm.

The fully articulated main rotor had collective and cyclic control. Spherical bearings at the cuff allowed for limited flapping and the attachment hinge allowed for lead/lag motion. The 2-bladed tail rotor had collective control and lead/lag hinges. The helicopter was attached to a 6-component balance for the measurement of the forces and moments. Space constraints dictated that the balance assembly was located below the fuselage, i.e. exposed to the external flow field. Initial concerns that the roll moment range of the small balance may have been exceeded were addressed by allowing the model to rotate on a bearing about the balance longitudinal axis. Appropriate hard stops were included to limit the allowable roll angle range.

A 2-stroke 50 size OS Max glow plug piston engine was used to drive the helicopter rotor through the standard clutch assembly. Fuel was supplied by a header tank arrangement located outside of the test section.

The helicopter model was fitted with a tachometer and potentiometer to measure rotor speed and blade azimuth position. The default RC coupling between the throttle (RPM) and the collective pitch angle caused the rotor speed to differ for different thrust levels. Similar fluctuations may be expected in response to the control system outputs to maintain the constant thrust levels required for the tests. The main rotor test speed was from 1000 - 1400 RPM yielding tip speeds of 70 – 97 m/s and tip Reynolds number of 180 000 – 260 000. This represented the range across the various thrust coefficients used across the whole test series. Typical rotor speed variations within a test were of the order of $\pm 5\%$ about the mean. This was due mostly to ambient wind changes that altered conditions in the test section.

The azimuth signal deteriorated steadily throughout the test and eventually required replacement. This was partly due to the hostile environment in close proximity to the 2-stroke engine exhaust

The model had been procured for a separate test series that did not require full definition of the rotor and it was not fitted with feedback transducers for the blade position. The collective and cyclic inputs were determined by calibration of the commanded signal and the measured static angles. The tip had to be estimated optically. It is accepted that these factors introduced significant uncertainty regarding comparisons with CFD but, nonetheless, the exercise may still be used to illustrate the merits and limitations of the approach.

The earthed part of the balance was attached to a variable pitch mechanism, which allowed for the active control required during trimmed flight for the helicopter. This pitch control mechanism was mounted on top of a stiff faired vertical strut centrally located in the test section (Figure 1).

The helicopter model was mounted to the balance assembly using rubber dampers which proved essential to eliminate ground resonance effects.

The helicopter flow field measurements were performed with a rapid response (embedded transducers) hemispherical tipped 5-hole probe.

The wind tunnel's integral overhead XYZ ϕ traverse system (Figure 1) was used to support and position the probe tip at the required longitudinal, lateral, and vertical locations relative to the helicopter for the tests. The probe was mounted to the end of an offset strut that was attached to the roll axis. This allowed the probe to be supported away from the traverse structure which reduced support interference effects. The maximum vertical position of the probe was some distance below the main rotor to reduce the possibility of a collision with the main rotor blades. The lateral cyclic range and roll angle range of the model helicopter also had to be considered. The minimum clearance for these tests was 137mm (2.8 chords) for zero pitch and roll attitude of the helicopter.

The 6-component strain gauge balance measured the aerodynamic forces on the model and the fuselage pitch and roll angles were measured by potentiometers. A computer was used to control the RC helicopter by supplying analogue control signals to the control inputs on the radio which were transmitted to the helicopter. The standard RC receiver was used with an external power supply. The model was free to roll and was controlled to a specified roll angle, using lateral cyclic.

Software control loops used feedback from the balance and attitude potentiometers to drive the control hardware to achieve trimmed flight for each case according to the arrangement in Table 1. The hover tests were performed at zero roll angle. A relatively high control loop frequency was required for the lateral cyclic due to the model being free to roll. This channel was operated off a separate hardware system with an update frequency of about 35 Hz, which proved adequate. The remaining control loops were less critical and operated at 10 to 15 Hz. The tethered nature of the support system meant that the attitude response had to be provided by the support system. The pitch motion was supplied by a motor and there was no yaw motion allowed.

For the forward flight tests, the helicopter was continuously trimmed to a specified thrust and zero moments about the mrc using the full control system. The hover tests were performed at a zero roll angle and angle of attack which represents an out of trim

condition for the lateral components. In both cases the lateral cyclic underwent rapid excursions as required to maintain the commanded roll angle.

Table 1: Helicopter control architecture

Helicopter channel	Feedback signal
Main rotor collective	Net lift force
Tail rotor collective	Net yaw moment about mrc
Longitudinal cyclic	Net drag force
Roll angle	Net side force
Lateral cyclic	Roll angle
Pitch angle	Net pitch moment about mrc
Throttle	Main rotor RPM

The origin of the coordinate system was the centre of the pivot point on the helicopter support system. A negative x position refers to downwind distance. A negative y position refers to port side location. A positive z position refers to distance above the origin. Note that the main rotor was located 487mm above the pivot point.

A pseudo thrust coefficient was used which is based on the net lift force in the wind axis system. The typically small variations in the tpp from the horizontal meant that this effectively approximated C_T :

$$C'_T = \frac{f l_w}{\pi A (\omega R)^2} \approx C_T$$

The forces and moments refer to net loads, i.e. the effects of model mass have been removed and the moments have been transferred to the required mrc for the helicopter.

Numerical Method

The three-dimensional helicopter flow field was computed with a commercial CFD code, STAR-CD (CD-Adapco) in hover and trimmed forward flight. A first order accurate, unsteady, viscous computation was achieved with numerical solution of the Reynolds Averaged Navier-Stokes equations and relative motion between tail rotor, main rotor and helicopter fuselage. Density variations were modelled.

Individual grids were generated about the tail rotor, main rotor and the fuselage. STAR-CD version 3.2 did not accommodate overlapping grids. The rotor grids had to be provided for within the bounding grid that included the fuselage. Connectivity between relatively moving grids was achieved with an "arbitrary sliding interface". Aero-elastic effects were not modelled and rotor coning was not taken into account. The main rotor blades were modelled in the main rotor tip path plane. The main rotor tip path

plane, main and tail rotor collective, longitudinal, lateral cyclic inputs and fuselage orientation were determined from the wind tunnel tests and were used to prescribe the motion of the blades as a function of azimuth.

The wind tunnel ground plane was modelled in hover but not in forward flight. The remaining boundaries on the computational domain were modelled as static pressure boundaries.

Size of the computational domain was limited by dynamic memory available on the single computer used to generate the CFD model. CFD models are currently limited to approximately 4.0 million grid points at CSIR. Transient simulations with mesh movement require all volumes on relatively moving/sliding boundaries to reside on a single node during parallel computation. The time taken for a single node to execute the motion of the blades, and to compute the flow field within the moving volumes, was the limiting factor in terms of total simulation time.

Results for the CFD models were extracted after (approximately) 20 revolutions of the main rotor due to the long simulation times. While this was not sufficient to achieve perfectly periodic results, the interim results presented here will serve to evaluate the potential of experimental data from RC helicopters for the validation of computed flow fields.

Instrumentation, Data Acquisition and Control Systems

The 5-hole probe pressure transducers were piezoresistive microphones (ENDEVCO Model 8507C-2) with a 2 psi pressure range. The tube length from the probe tip to the transducers was ~100mm. The frequency response of the 5-hole probe is shown in Figure 2 for one of the ports which is representative of the whole probe.

The 5-hole probe pressure transducers were scanned with a sample and hold card at 2048 Hz. This frequency was necessary to effectively discretize the signal. The blade passing event was of the order of 100 Hz which should not be significantly affected by the probe dynamic response. The typical pressure fluctuations encountered close to the rotor blades are shown in Figure 3. A sample trace was corrected by applying the inverse of the probe response transfer function. The required correction was found to be negligible (Figure 4) and was therefore not applied to the test data.

The 5-hole probe was calibrated using multivariable polynomial algorithms across sectors defined by the pressure magnitudes (Ref 2). The accuracy of the calibration is shown in Table 2.

Table 2: 5-hole probe calibration accuracy

Parameter	Uncertainty (95%)
Vmag	1.5 m/s
α	2.8 °
β	3.0 °

Calculated angles of magnitude greater than 60° were excluded from results for these tests. This has implications for measurements of hover flow fields when the probe is positioned outside, or near the boundary, of the downwash zone where high angles and reverse flow are common.

Test Procedure

The helicopter was started and brought to a hover condition using a combination of manual and automatic control. The wind tunnel was then started and accelerated to speed while the control loops trimmed the helicopter. When the conditions were satisfactorily stable, sampling of the 5-hole probe data commenced for a specified time period at each point in a defined grid pattern.

In post test analysis, the time history for the grid scans was reconstructed by correlating the signals with the main rotor azimuth position signal. Multi-order trigonometric functions were used to curve-fit the data from which the results at any azimuth could be determined. For the hover data this could be achieved with relatively low order functions (Figure 5). The high gradients in the trailing vortex pattern at the boundaries of the downwash could not be measured due to the presence of reverse flow in these regions. However for the forward flight tests, the wake vortices could be measured due to the superposition of the free stream velocity which mitigated the flow reversal issue. This produced significant gradients that required higher order functions to be used in the curve fitting process (Figure 6). Note that here we are primarily interested in the steady state periodic response and therefore transients due to external factors should be ignored.

The measurements were taken in three planes on the port side of the helicopter only. The origin for the probe coordinates was the pivot point of the helicopter in the pitch plane. This was located some 487mm below the main rotor. The highest coordinate used for the scans was z=350mm which is equivalent to 137mm below the rotor disk. Three planes were scanned; they were located at X/R = 0, X/R = -0.61, and X/R = 1.22. This roughly located the planes in line with the main rotor, in line with the tail rotor, with a third midway between these two (see Figure 7).

Table 1. Test conditions.

	Hover	Forward Flight
x/R	0	0; -0.61; -1.22
C_T/σ	0.032	0.043
μ	0	0.052
RPM	1363; 1060	1080
Grid; Ymm x Zmm	300x300	500x300
F, Hz	2000	2000
Time per point	1s	0.5s

Test Results

Hover

The 5-hole probe has a limited cone of validity outside of which results are meaningless. In the hover cases, excessive angles and flow reversals are located in the vicinity of the shear layer between the downwash and the ambient air. Also whenever the velocities are low, turbulence can easily result in angles that the probe cannot resolve. A similar condition occurs far inboard of the rotor disk, near the fuselage where the induced velocity is low and may even reverse. When these events form a significant percentage of the time trace the data from the probe cannot be trusted, which limits the reliable hover data to well within the induced downwash region.

Time averaged flow field results are presented for the hover case in Figures 8 and 9. The wind tunnel data was truncated where flow reversal effects became significant. The general correlation is fair but the steep outer gradient of the downwash measured in the wind tunnel was not reproduced in the CFD data. This is considered primarily due to insufficient grid density across the downwash shear layer. One of the benefits of comparisons such as this is to provide insight and guidance on the distribution of the finite number of cells available for CFD models.

The smaller magnitude down wash from the CFD run was reflected in a lower value of integrated momentum lift when compared to the wind tunnel data. This should not be surprising considering the indirect calibration method (commanded angle) that was used to determine the amount of collective in the wind tunnel experiment. More fair comparisons will be possible if the RC helicopter hub were instrumented to provide the actual blade position.

The reconstructed pressure signal correlated with azimuth position is shown in Figure 10. The variability in the wind tunnel data exposed some of

the challenges and limitations of the wind tunnel experiment set up. The variability is caused by ambient wind changes that affect the test section flow in the open return wind tunnel. In addition, the attitude about the unconstrained roll axis is maintained by a control system linked to lateral cyclic. Control response to disturbances from the commanded attitude, coupled with the roll attitude of the helicopter, would have introduced a variance in the separation between the rotor blades and the probe tip. This would be manifest as variations in the pressure pulses sensed by the probe. This is further aggravated by the low thrust coefficient.

It may also be seen from Figure 10 that two of the blades are more highly loaded than the other two blades. Although care was taken to track the blades using a strobe light, a tracking error was frequently present.

A representative signal trace at a fixed point was extracted from this data and is shown in Figure 11. The blade passing event is captured in both cases although there is a disturbing phase difference between the CFD and the wind tunnel. This cannot be attributed to the probe frequency response (Figure 2) and is likely due to belt slip or calibration error regarding the azimuth potentiometer. The deteriorating azimuth signal had to be reconstructed with a triangular wave anchored at the phase shift nodes which could then be used to correlate the individual signals to allow the dynamic environment to be reconstructed from the discretely sampled data.

The comparison in Figure 11 does suggest that the amplitude of the pressure pulses from the blades are slightly underpredicted. Also, the CFD peak pressure leads the blade, which is somewhat curious, however the phase wrapped data exhibited a small step whereas a fully converged solution would be "smoothly periodic". One of the questions to be answered in the STAR-CD model is how faithfully the sliding interface required for the rotor transmits the rotor effect into rest of the domain.

The data quality is showing impressive potential in spite of the signal amplitude only being 0.5% of the transducer range. This is, however, an undesirable condition because the relative impact of temperature changes, ambient wind changes (open return wind tunnel), electrical noise, etc becomes more significant. Methods to reduce, or compensate for, these effects should be sought to improve the Signal to Noise ratio.

Forward Flight

A similar approach was followed for the forward flight flow field measurements. The 5-hole probe was supported at 36.5° up from the horizontal to reduce the local flow angularity at the probe tip (Figure 1). The results were converted to the wind axes reference system and the corresponding data was extracted from the CFD solution.

A comparison between the wind tunnel measurements and the CFD solution is shown in Figures 12 to 15. The plots have been made using a constant colour scale to highlight differences. Similar trends are found in the results but the amplitude of the pressures in the CFD solutions is significantly lower than the wind tunnel data. The 4 per rev blade passing event is clear in both data sets; the CFD solution being very crisp and the wind tunnel data appearing to be smeared. Again, two blades are working harder than the other two in the wind tunnel data sets. The low pressure region in Figure 15a corresponds to the path of the developing trailing vortex and contained fluctuating flow structures that were hidden when the scales were fixed for comparison purposes.

It is felt that the significantly lower pressures in the CFD results are closely related to the lack of properly defined rotor blade setting angles from the experiment. This is at odds with the relatively good correlation between the wind tunnel and CFD for the hover test case. A similar correlation would be expected from the forward flight comparisons. cursory inspection of the forward flight CFD solution in the v-w plane (Figure 16) indicated more activity on the starboard side which is consistent with "out of trim" lateral cyclic.

Note that the support system for the RC helicopter was unstable in roll. Any rotation of the model about the roll axis would shift the RC helicopter cg away from through the centre line of the balance. This would produce a roll moment about the bearing arrangement on the balance roll axis. Unless acted upon by an external force, the roll angle would increase until the roll dead stops. So a net aerodynamic roll moment is required for the RC helicopter to maintain a steady non-zero roll angle in simulated flight.

The presence of the 4 per rev pressure pulse changes from spanning most of the scan plane at $x/R=0$, to around half the scan plane at $x/R=-0.61$, to being virtually undetected at $x/R = -1.22$. This is consistent with the location of the main rotor blades with respect to the measurement planes.

The time averaged pressure plots at the $x/R = -0.61$ station show the development of a low pressure region corresponding to the trailing vortex.

Conclusions

The scatter in the azimuth signal did not allow the curve fitting algorithm to track significant transients that were noticed in the data. In these cases, the curve fit provided an average representation which reduced the magnitudes of the peaks. So although the probe was demonstrated to be capable of detecting the frequencies and amplitudes present in the wake, these could not always be adequately correlated with the azimuth signal for the post test data reconstruction. A higher quality azimuth signal is required, probably an optical encoder.

With sufficient care, the rapid response probe used for these tests is considered capable of being used to generate good quality reference data for computational fluid dynamic code validation.

Future work along these lines would require that the helicopter hub be instrumented for the actual collective and cyclic angles experienced by the blades to eliminate the approximations that were made in the current investigation.

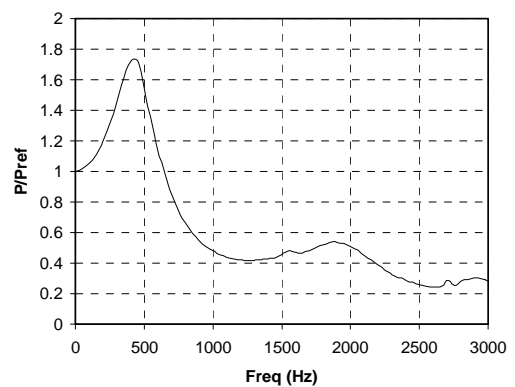
Electric motors should be used to power the helicopter to avoid high temperatures and oil deposits interfering with the test equipment.

Future work would benefit from an idealised approach where a more constrained system is used to eliminate some of the undesirable variability in the test data. This is not a hindrance to CFD validation – all that is required is that the numerical models must duplicate the level of constraint imposed.

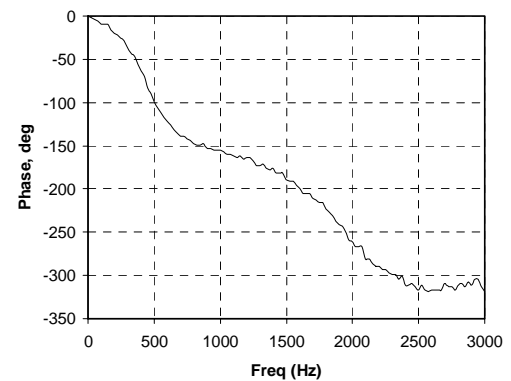
For adequate reference data more stable tunnel conditions are required, particularly at low advance ratios and thrust coefficients. In large open circuit return facilities this means that increased resistance is required in the form of mesh screens at the inlet to smooth out the effects of ambient wind fluctuations.



Figure 1 Installation in the wind tunnel



a) amplitude



b) phase

Figure 2 5-hole probe frequency response

References

- [1] Denton, T.J., Martins, J.C.F., Ratner, G.R., and Skinner, P.J., "Experimental Characterisation and Comparison of a Model Helicopter Rotor Tip Vortex and Fixed Wing Tip Vortex", 29th European Rotorcraft Forum, Germany
- [2] Gerner, A.A. and Maurer, C.L., "Calibration of Seven-Hole Probes Suitable for High Angles In Subsonic Compressible Flows", USAFA-TR-81-4

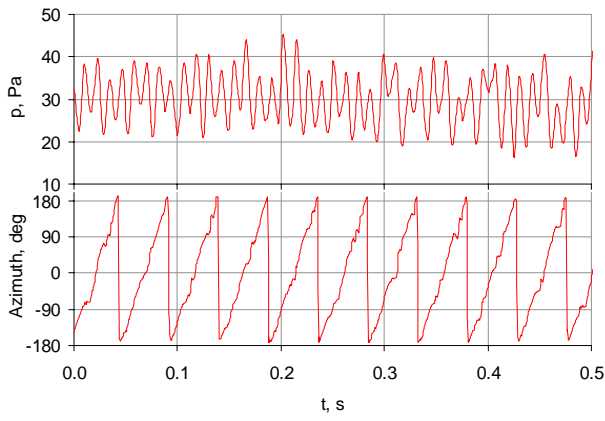


Figure 3 Typical 4 per rev signal trace

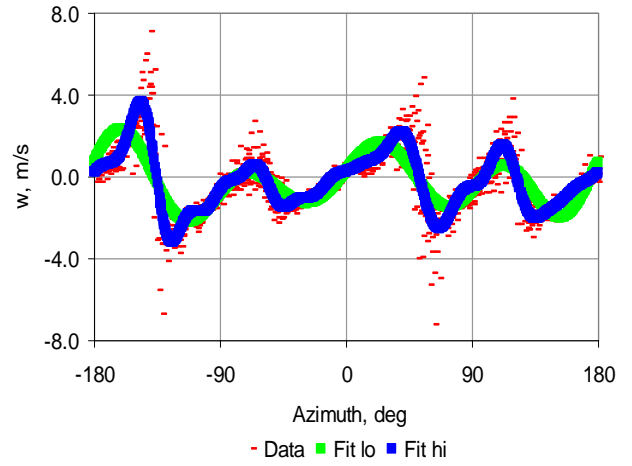


Figure 6 Wake vortex encounters during forward flight requiring higher order functions

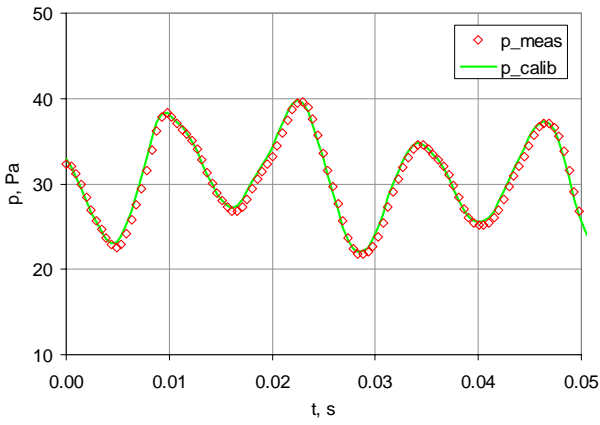


Figure 4 Effect of 5-hole probe frequency response function

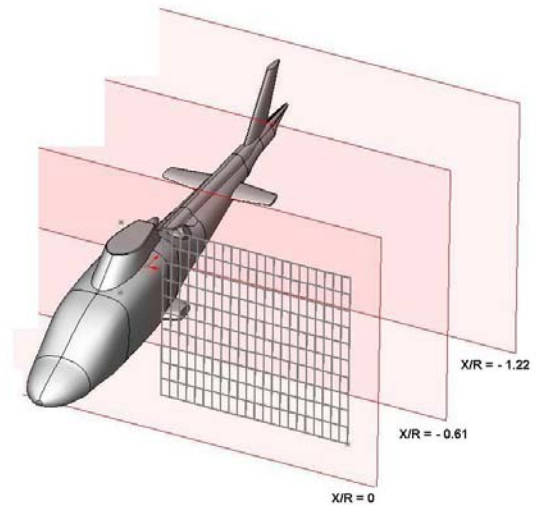


Figure 7 Location of scanning planes on port side of helicopter

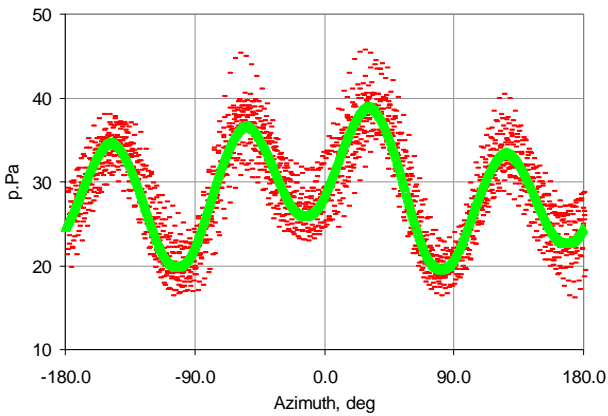
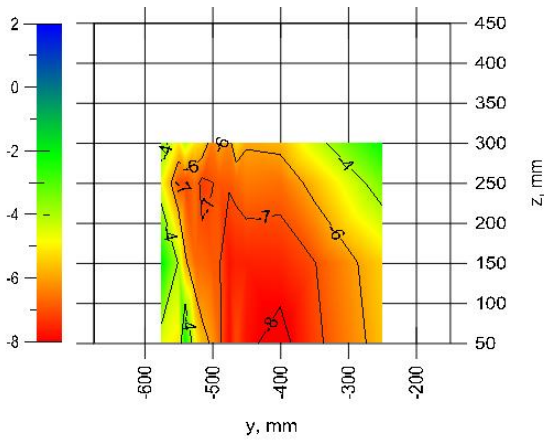
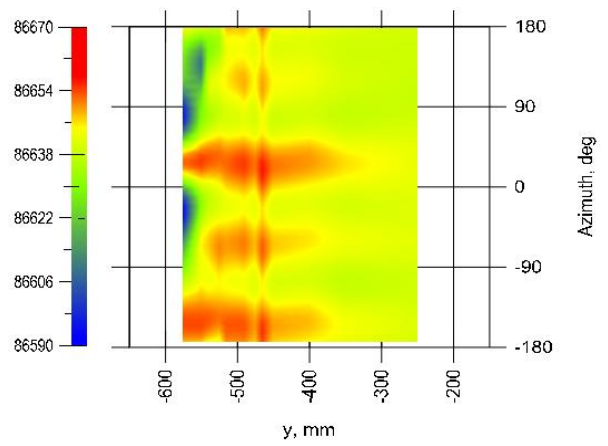


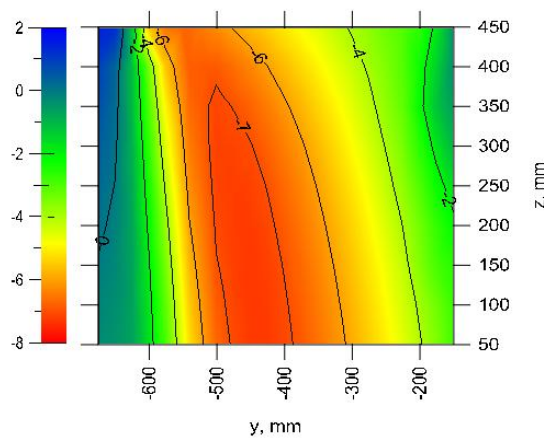
Figure 5 Typical blade pressure pulses in hover



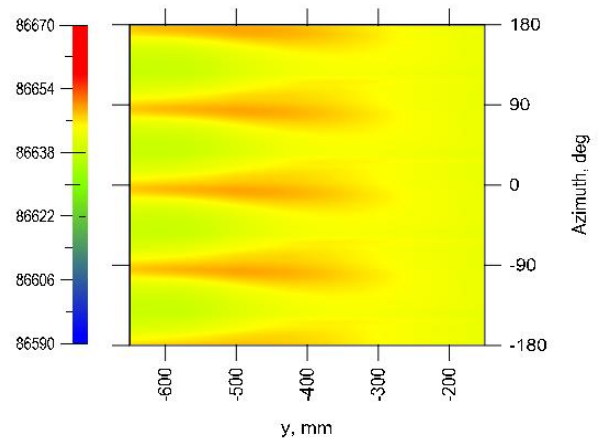
a) Wind tunnel



a) wind tunnel



b) CFD



b) CFD

Figure 8 Time averaged w component (m/s) flow fields for similar thrust levels in hover

Figure 10 Comparison of pressure traces (ps, Pa) for hover $C_T/\sigma = 0.032$; $x = 0\text{mm}$; $z = -187\text{mm}$

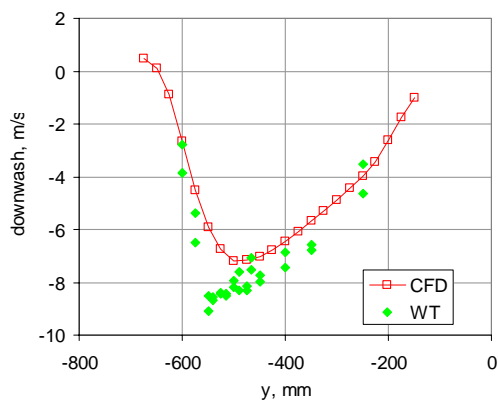


Figure 9 Average downwash for hover; $C_T/\sigma = 0.032$; $x = 0\text{mm}$, $z = -187\text{mm}$

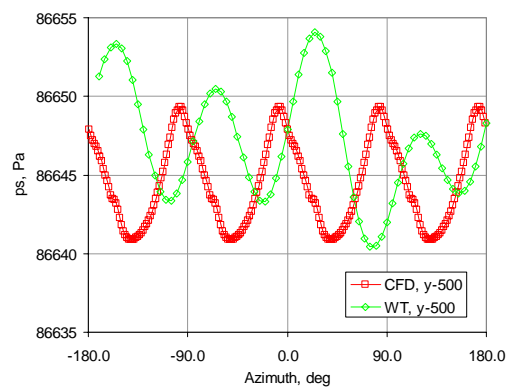
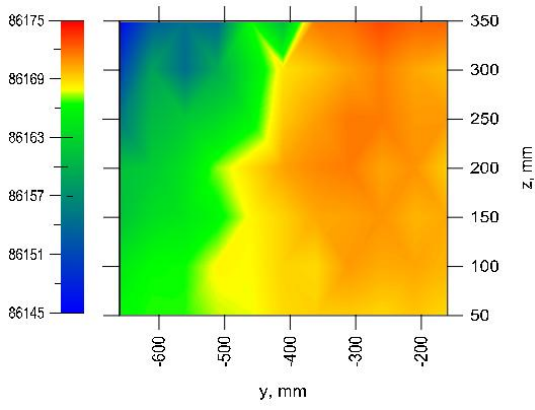
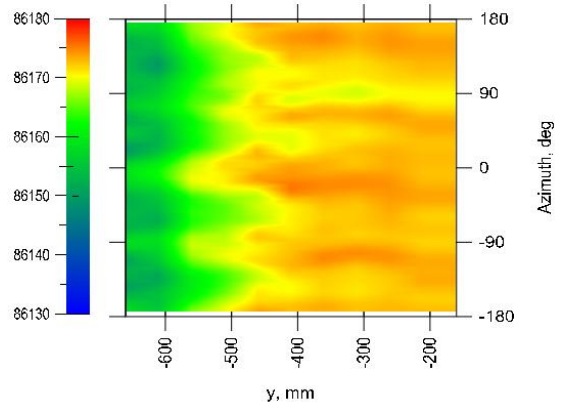


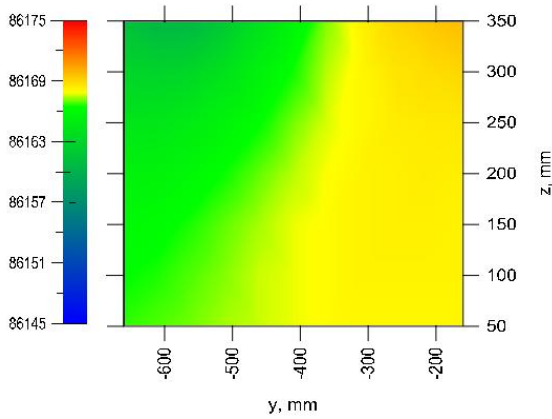
Figure 11 Pressure traces (ps, Pa) at fixed lateral location for hover; $C_T/\sigma = 0.032$; $x = 0\text{mm}$; $y = -500\text{mm}$, $z = -187\text{mm}$



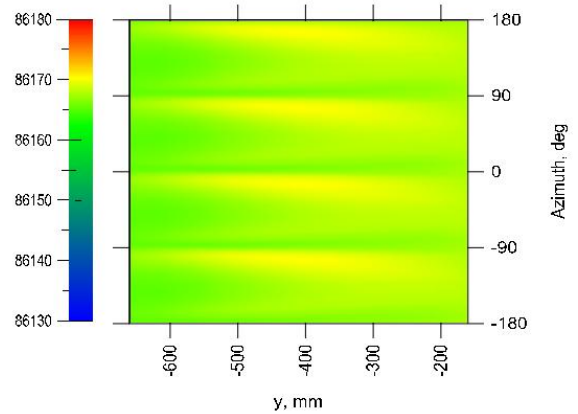
a) wind tunnel



a) wind tunnel



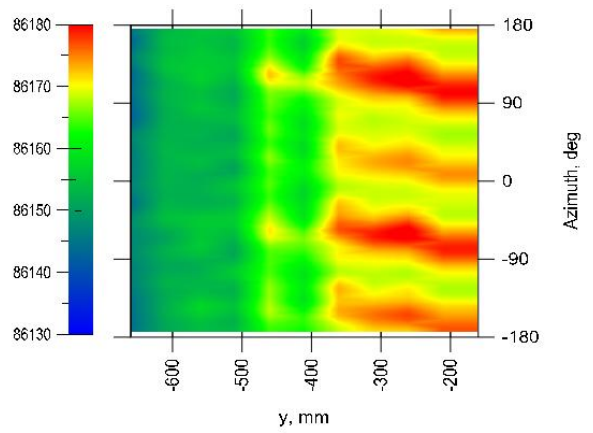
b) CFD



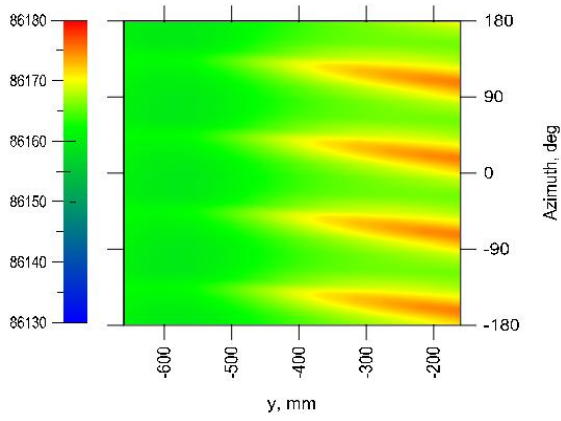
b) CFD

Figure 12 Time averaged ps (Pa) in vertical measurement plane; $x/R = -0.61$; $C_T/\sigma = 0.043$; $\mu = 0.052$

Figure 13 Comparison of pressure traces (ps, Pa) for forward flight $C_T/\sigma = 0.043$; $\mu = 0.052$; $xR = 0$; $z = -187\text{mm}$ (below main rotor)



a) wind tunnel



b)CFD

Figure 14 Comparison of pressure traces (ps, Pa) for forward flight $C_T/\sigma = 0.043$; $\mu = 0.052$; $xR = -0.61$; $z = -187\text{mm}$ (below main rotor)

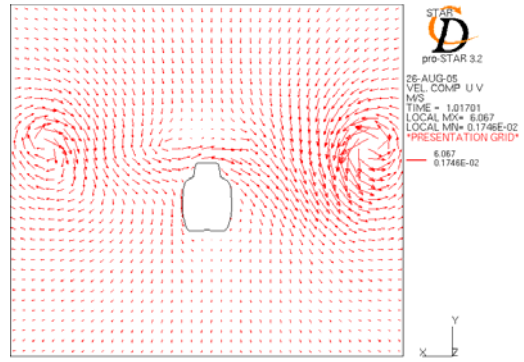
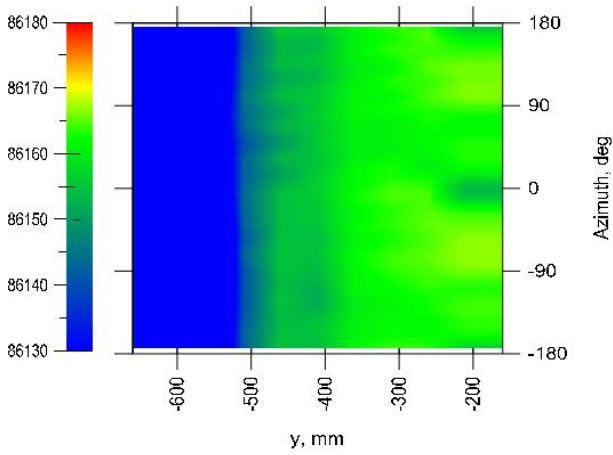
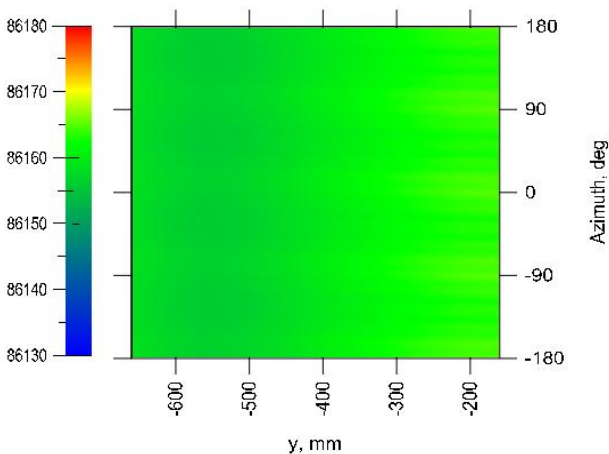


Figure 16 CFD forward flight result showing significant asymmetry that suggests incorrect lateral cyclic setting



a) wind tunnel (scale fixed deliberately)



b) CFD

Figure 15 Comparison of pressure traces (ps, Pa) for forward flight $C_T/\sigma = 0.043$; $\mu = 0.052$; $xR = -1.22$; $z = -187\text{mm}$ (below main rotor)